

Stochastic sampling of quadrature grids for the evaluation of vibrational expectation values

Pablo López Ríos,^{1,2,*} Bartomeu Monserrat,^{2,3} and Richard J. Needs²

¹Max-Planck Institute for Solid State Research, Heisenbergstraße 1, 70569 Stuttgart, Germany

²Theory of Condensed Matter Group, Cavendish Laboratory, J. J. Thomson Avenue, Cambridge CB3 0HE, UK

³Department of Physics and Astronomy, Rutgers University, Piscataway, New Jersey 08854-8019, USA

(Dated: October 9, 2018)

The *thermal lines* method for the evaluation of vibrational expectation values of electronic observables [B. Monserrat, *Phys. Rev. B* **93**, 014302 (2016)] was recently proposed as a physically motivated approximation offering balance between the accuracy of direct Monte Carlo integration and the low computational cost of using local quadratic approximations. In this paper we reformulate thermal lines as a stochastic implementation of quadrature grid integration, analyze the analytical form of its bias, and extend the method to multiple point quadrature grids applicable to any factorizable harmonic or anharmonic nuclear wave function. The bias incurred by thermal lines is found to depend on the local form of the expectation value, and we demonstrate that the use of finer quadrature grids along selected modes can eliminate this bias, while still offering a $\sim 30\%$ lower computational cost than direct Monte Carlo integration in our tests.

I. INTRODUCTION

First-principles studies of solid state systems typically use the Born-Oppenheimer approximation¹ to simplify the task of solving the Schrödinger equation of the system by separating the electronic and nuclear degrees of freedom. Density functional theory (DFT)² is the *de facto* standard method for solving the electronic problem in crystalline systems, allowing the numerical evaluation of a large number of relevant properties of materials at a relatively low computational cost. The approximate nature of density functionals proves problematic in some cases, and more accurate, computationally costly methods such as the *GW* approximation^{3,4} or quantum Monte Carlo^{5,6} can be used instead for the evaluation of ground-state observables.

Many electronic properties can usually be evaluated accurately within the static lattice approximation, in which the electronic problem is solved neglecting the effects of nuclear motion entirely. However, zero-point quantum corrections play a crucial role in systems containing light elements, and the description of thermal effects requires the inclusion of vibrations in all systems. The harmonic approximation⁷⁻⁹ enables the inclusion of nuclear motion for the calculation of the total energy at small computational cost. Although this approach is very accurate for most systems, there are notable exceptions including systems with light atoms,¹⁰ those involving weak bonding between atoms,¹¹ those at high temperature,¹² or those near structural phase transitions.¹³ Anharmonic approximations¹⁴⁻¹⁹ exist that are able to overcome these limitations at an additional computational cost.

Vibrational corrections to electronic properties other than the energy can be calculated as the expectation value of the property of interest with respect to the vibrational harmonic or anharmonic nuclear wave function. Literature examples of such calculations include thermal averages of the electronic band structure,²⁰⁻²² the dielectric function,²³⁻²⁶ the chemical shielding tensor,²⁷⁻³¹ the x-ray absorption near-edge structure,³¹ or the contact hyperfine interaction.^{32,33} These vibrational averages have traditionally been computed using either a quadratic expansion of the electronic observ-

able around its equilibrium value, or Monte Carlo integration. The former approach is computationally advantageous, but neglects multi-phonon terms in the electron-phonon interaction. The latter approach is computationally costly, but multi-phonon terms are correctly captured. The recent demonstration that multi-phonon terms can be important in a number of cases³⁴⁻³⁷ has motivated the development of the thermal lines method,³⁸ which can partially capture multi-phonon terms at a smaller computational cost than Monte Carlo integration.

The thermal lines method was proposed as a physically-motivated approximation to the evaluation of vibrational expectation values of electronic observables, offering faster statistical convergence than Monte Carlo integration and better accuracy than the quadratic approximation, but its bias has not yet been quantified. In the present paper we analyze the bias of the thermal lines method, and use this analysis to propose an integration method based on the stochastic sampling of quadrature grids constructed from the vibrational wave function. The bias in our proposed method is controlled by the number of grid points, reducing to thermal lines for a two-point grid and to Monte Carlo integration in the infinite-point limit. Our results indicate that thermal lines (two-point grids) are capable of accurately incorporating the effects of multi-phonon terms in most calculations of vibrational expectation values. However, we find that the bias incurred by thermal lines is not negligible for observables with a strong non-quadratic behavior, and multiple point grids are required in order to obtain accurate expectation values in these cases.

The rest of this paper is structured as follows. In section II we provide the theoretical background and describe the relevant methods for the evaluation of vibrational expectation values. The bias in the thermal lines method is analyzed in section III. In section IV we formulate and test one-dimensional quadrature grids, and in section V we discuss the use of these grids in multi-dimensional Monte Carlo sampling for realistic examples of vibrational averages of electronic observables. Finally, we summarize our findings in section VI. Hartree atomic units ($\hbar = |e| = m_e = 4\pi\epsilon_0 = 1$) are used throughout.

II. VIBRATIONAL CALCULATIONS

In computer simulations, crystalline solids are represented by supercells containing N nuclei and N_e electrons subject to periodic boundary conditions. Within the Born-Oppenheimer approximation, the electronic Hamiltonian $\hat{H}_{\text{el}}(\mathbf{R})$ parametrically depends on the nuclear positions \mathbf{R} , and the resulting electronic energy $E_{\text{el}}(\mathbf{R})$, in which we include nucleus-nucleus interactions, acts as an external potential in the vibrational Hamiltonian,

$$\hat{H}_{\text{vib}}(\mathbf{R}) = - \sum_{\alpha=1}^N \frac{1}{2m_{\alpha}} \nabla_{\alpha}^2 + E_{\text{el}}(\mathbf{R}). \quad (1)$$

Without loss of generality we will assume that $E_{\text{el}}(\mathbf{R}_0) = 0$, where \mathbf{R}_0 is the equilibrium nuclear configuration. The nuclear motion problem has three translational degrees of freedom which can be eliminated, and $n = 3N - 3$ vibrational degrees of freedom.

It is convenient to work in terms of normal-mode coordinates $\mathbf{u} = \{u_i\}_{i=1}^n$, which are the real-valued linear combinations of nuclear displacements under which the dynamical matrix is diagonal.⁷⁻⁹ We replace the phonon branch ν and wave vector \mathbf{q} , which are the standard normal mode quantum numbers, by a single index i for notational convenience. Note that $\mathbf{u} = \mathbf{0}$ at the equilibrium nuclear configuration \mathbf{R}_0 . In these coordinates, Eq. 1 reads

$$\hat{H}_{\text{vib}}(\mathbf{u}) = -\frac{1}{2} \sum_{i=1}^n \frac{\partial^2}{\partial u_i^2} + E_{\text{el}}(\mathbf{u}). \quad (2)$$

The ground-state vibrational wave function $\Phi(\mathbf{u})$ determines the zero-temperature quantum vibrational properties of the system, and can be obtained by solving the vibrational Schrödinger equation, $\hat{H}_{\text{vib}}(\mathbf{u})\Phi(\mathbf{u}) = E_{\text{vib}}\Phi(\mathbf{u})$.

Under the harmonic approximation, the electronic energy is assumed to take the form $E_{\text{el}}(\mathbf{u}) = \sum_i \frac{1}{2} \omega_i u_i^2$, where the harmonic frequency of the i th normal mode ω_i can be obtained by differentiating the electronic energy, either using finite differences^{39,40} or methods such as density functional perturbation theory,⁴¹ with respect to u_i . The harmonic approximation results in a wave function of the form $\Phi^{(\text{har})}(\mathbf{u}) = \prod_{i=1}^n \phi_i^{(\text{har})}(u_i)$, where

$$\phi_i^{(\text{har})}(u_i) = \left(\frac{\omega_i}{\pi}\right)^{1/4} \exp\left(-\frac{1}{2}\omega_i u_i^2\right). \quad (3)$$

Various methods for dealing with anharmonic vibrational Hamiltonians exist which lift the restriction on the form of the electronic energy,¹⁵⁻¹⁹ but all these methods assume that the wave function can be factored as a product of single-mode functions, $\Phi(\mathbf{u}) = \prod_{i=1}^n \phi_i(u_i)$. In our analysis we assume the use of a factorizable vibrational wave function.

We focus our present discussion on the zero-temperature limit for simplicity. Thermal effects can be trivially included by replacing the ground-state vibrational density Φ^2 with $\frac{1}{\mathcal{Z}} \sum_{\mathbf{s}} \Phi_{\mathbf{s}}^2 e^{\beta E_{\mathbf{s}}}$, where $\beta = (k_{\text{B}}T)^{-1}$ is the inverse temperature, \mathbf{s} identifies the vibrational excited state corresponding to

wave function $\Phi_{\mathbf{s}}$ and energy $E_{\mathbf{s}}$, and $\mathcal{Z} = \sum_{\mathbf{s}} e^{\beta E_{\mathbf{s}}}$ is the partition function of the system. We note that the ‘‘mean thermal line’’ approach for evaluating finite-temperature expectation values³⁸ remains applicable to our proposed method.

A. Vibrational expectation values

Knowledge of $\Phi(\mathbf{u})$ enables the evaluation of the expectation value of an electronic observable \hat{A} with respect to the vibrational density as

$$\langle A \rangle_{\Phi^2} = \int \Phi^2(\mathbf{u}) A(\mathbf{u}) d\mathbf{u}, \quad (4)$$

where $A(\mathbf{u}) = \Phi^{-1}(\mathbf{u}) \hat{A} \Phi(\mathbf{u})$ is the local value of the observable at nuclear configuration \mathbf{u} . Under the assumption that $A(\mathbf{u})$ is a smooth function of its arguments, it is useful to express it as a power expansion,

$$\begin{aligned} A(\mathbf{u}) = & A(\mathbf{0}) + \sum_i^n a_i^{(1)} u_i + \sum_{i \leq j}^n a_{ij}^{(2)} u_i u_j \\ & + \sum_{i \leq j \leq k}^n a_{ijk}^{(3)} u_i u_j u_k + \dots, \end{aligned} \quad (5)$$

where $a_i^{(1)}$, $a_{ij}^{(2)}$, $a_{ijk}^{(3)}$, etc., are linear expansion coefficients. It should be noted that the approximations involved in solving the vibrational Schrödinger equation are distinct from those applied to $A(\mathbf{u})$; namely, the use of the harmonic wave function does not imply that expectation values are assumed to be quadratic functions of \mathbf{u} (or *vice versa*), and the use of a factorizable wave function without explicit phonon-phonon correlations does not imply neglecting multi-mode contributions from Eq. 5 (or *vice versa*).⁴²

1. The quadratic approximation

If $\Phi(\mathbf{u})$ is symmetric, such as in the harmonic approximation, substituting Eq. 5 into Eq. 4 results in the cancellation of all contributions involving odd powers of a normal-mode coordinate,

$$\begin{aligned} \langle A \rangle_{\Phi^2} = & A(\mathbf{0}) + \sum_i^n a_{ii}^{(2)} \langle u_i^2 \rangle_{\Phi^2} + \sum_{i \leq j}^n a_{iijj}^{(4)} \langle u_i^2 u_j^2 \rangle_{\Phi^2} \\ & + \sum_{i \leq j \leq k}^n a_{iijjkk}^{(6)} \langle u_i^2 u_j^2 u_k^2 \rangle_{\Phi^2} + \dots, \end{aligned} \quad (6)$$

and since Φ^2 is factorizable, Eq. 6 reduces to a linear combination of products of one-dimensional integrals. Neglecting fourth- and higher-order contributions to Eq. 6 yields the *quadratic approximation*,

$$\langle A \rangle_{\Phi^2} \approx A(\mathbf{0}) + \sum_i^n a_{ii}^{(2)} \langle u_i^2 \rangle_{\phi_i^2}, \quad (7)$$

where $a_{ii}^{(2)} = \frac{1}{2} \left(\frac{\partial^2 A}{\partial u_i^2} \right)_{\mathbf{u}=\mathbf{0}}$, and the one-dimensional integrals $\langle u_i^2 \rangle_{\Phi_i^2}$ can easily be calculated; in the harmonic approximation, $\langle u_i^2 \rangle_{\Phi_i^2} = (2\omega_i)^{-1}$.

2. Direct Monte Carlo integration

An unbiased estimate of the integral of Eq. 4 can be evaluated using Monte Carlo integration,

$$\langle A \rangle_{\Phi^2} \approx \frac{1}{M} \sum_{m=1}^M A(\mathbf{u}_m), \quad (8)$$

where $\{\mathbf{u}_m\}$ are M random vectors of normal-mode coordinates distributed according to $\Phi^2(\mathbf{u})$. This method, which we refer to as *direct Monte Carlo* in what follows, is exact in the limit $M \rightarrow \infty$, and requires no assumptions about the form of $A(\mathbf{u})$ or $\Phi(\mathbf{u})$. However, if the wave function is symmetric about $\mathbf{u} = \mathbf{0}$, $\Phi(\mathbf{u}) = \Phi(-\mathbf{u})$, it is advantageous to accumulate samples in $\{\mathbf{u}, -\mathbf{u}\}$ pairs in order to exactly remove odd-order contributions,

$$\begin{aligned} A^*(\mathbf{u}) &= \frac{1}{2} [A(\mathbf{u}) + A(-\mathbf{u})] \\ &= A(\mathbf{0}) + \sum_{i \leq j}^n a_{ij}^{(2)} u_i u_j \\ &\quad + \sum_{i \leq j \leq k \leq l}^n a_{ijkl}^{(4)} u_i u_j u_k u_l + \dots, \end{aligned} \quad (9)$$

resulting in reduced random noise and faster statistical convergence, while giving the correct expectation value since it is trivial that $\langle A(\mathbf{u}) \rangle_{\Phi^2} = \langle A^*(\mathbf{u}) \rangle_{\Phi^2}$. This sampling strategy, which we refer to as *symmetrized sampling*, was used in Ref. 38 for the ‘‘TL₂’’ variant of the thermal lines method, but it can be used to accelerate any Monte Carlo evaluation of the expectation value of \hat{A} with a symmetric wave function.

3. Thermal lines

Inspired by the mean value theorem for integrals, the thermal lines method³⁸ postulates that a good approximation to the expectation value of \hat{A} for a symmetric wave function is given by

$$\langle A \rangle_{\Phi^2} \approx \frac{1}{M} \sum_{m=1}^M A[\mathbf{u}_{\text{TL}}(\mathbf{S}_m)], \quad (10)$$

where $\{\mathbf{S}_m\}$ are M random n -dimensional vectors each of whose components takes the values $+1$ and -1 with equal probability, and $\mathbf{u}_{\text{TL}}(\mathbf{S})$ is a vector whose i th component is $S_i U_i$, where $U_i = \sqrt{\langle u_i^2 \rangle_{\Phi^2}}$.

The thermal lines method defines ‘‘special’’ points at which to sample the integrand, much in the spirit of special k -point methods for integrals over the Brillouin zone of a

crystal,^{43,44} or quadrature grids for integrals over the surface of a sphere,^{45,46} and uses Monte Carlo sampling of these points to efficiently deal with the high dimensionality of the integration volume. Although the effectiveness of thermal lines for the calculation of vibrational averages was demonstrated in Ref. 38, there was no formal analysis of the bias incurred by replacing Eq. 8 by Eq. 10. We present such analysis in section III.

We note that Monte Carlo sampling over thermal lines has been used to study the effects of electron-phonon coupling on the temperature dependence of the band gaps of a number of semiconductors within the *GW* approximation⁴⁷ and to study phonon-assisted optical absorption in BaSnO₃ using a hybrid DFT functional.⁴⁸ It has also been shown that, in the thermodynamic limit $n \rightarrow \infty$, a single thermal line delivers the exact thermal average $\langle A \rangle_{\Phi^2}$ without the need of Monte Carlo sampling. This thermal line is such that the sign S_i alternates between $+1$ and -1 when the coordinates u_i are ordered by increasing value of their associated harmonic frequencies ω_i .⁴⁹ Finally, we note that other methods in the same spirit as thermal lines have been used, for example in the study of superconducting hydrogen sulfides.⁵⁰

III. ANALYSIS OF THERMAL LINES

The distribution of normal-mode configurations \mathbf{u} sampled in Eq. 10 can be identified with the following probability density function,

$$\Phi_{\text{TL}}^2(\mathbf{u}) = \frac{1}{2^n} \prod_{i=1}^n [\delta(u_i - U_i) + \delta(u_i + U_i)], \quad (11)$$

where Φ_{TL} is the ‘‘thermal lines wave function’’. At $\mathbf{u}_{\text{TL}} = \{S_i U_i\}$, Eq. 5 becomes

$$\begin{aligned} A(\mathbf{u}_{\text{TL}}) &= A(\mathbf{0}) + \sum_{i=1}^n a_{ii}^{(1)} S_i U_i + \sum_{i \leq j}^n a_{ij}^{(2)} S_i S_j U_i U_j \\ &\quad + \sum_{i \leq j \leq k}^n a_{ijk}^{(3)} S_i S_j S_k U_i U_j U_k \\ &\quad + \sum_{i \leq j \leq k \leq l}^n a_{ijkl}^{(4)} S_i S_j S_k S_l U_i U_j U_k U_l + \dots \end{aligned} \quad (12)$$

The expectation value of products of powers of S for different modes factorizes into products of single-mode expectation values, e.g., $\langle S_i^\beta S_j^\gamma \rangle = \langle S_i^\beta \rangle \langle S_j^\gamma \rangle$ for $i \neq j$, and each of these is zero if the exponent is odd and unity if the exponent is even. The expectation value of \hat{A} under the thermal lines wave function is therefore

$$\begin{aligned} \langle A \rangle_{\Phi_{\text{TL}}^2} &= A(\mathbf{0}) + \sum_i^n a_{ii}^{(2)} U_i^2 + \sum_{i \leq j}^n a_{iijj}^{(4)} U_i^2 U_j^2 \\ &\quad + \sum_{i \leq j \leq k}^n a_{iijjkk}^{(6)} U_i^2 U_j^2 U_k^2 + \dots, \end{aligned} \quad (13)$$

which agrees with the quadratic approximation to second order, but includes higher-order multi-mode contributions. Subtracting Eq. 13 from Eq. 6 and substituting $U_i^2 = \langle u_i^2 \rangle_{\Phi^2}$, the bias in the thermal lines expectation value is

$$\begin{aligned} \langle A \rangle_{\Phi^2} - \langle A \rangle_{\Phi_{\text{TL}}^2} &= \sum_i^n a_{iii}^{(4)} (\langle u_i^4 \rangle_{\Phi^2} - \langle u_i^2 \rangle_{\Phi^2}^2) \\ &+ \sum_i^n a_{iiii}^{(6)} (\langle u_i^6 \rangle_{\Phi^2} - \langle u_i^2 \rangle_{\Phi^2}^3) \\ &+ \sum_{i<j}^n a_{iiij}^{(6)} (\langle u_i^4 \rangle_{\Phi^2} - \langle u_i^2 \rangle_{\Phi^2}^2) \langle u_j^2 \rangle_{\Phi^2} \\ &+ \sum_{i<j}^n a_{ijjj}^{(6)} \langle u_i^2 \rangle_{\Phi^2} (\langle u_j^4 \rangle_{\Phi^2} - \langle u_j^2 \rangle_{\Phi^2}^2) \\ &+ \mathcal{O}(u^8). \end{aligned} \quad (14)$$

It should be noted that the bias in the quadratic approximation includes all fourth- and higher-order terms in Eq. 6, while Eq. 14 shows that the bias in thermal lines arises solely from terms of fourth or higher order in which all index values appear an even number of times. Therefore the bias in thermal lines expectation values can typically be expected to be smaller than that for the quadratic approximation.

The variance of the values of $A(\mathbf{u})$ encountered during Monte Carlo integration determines the statistical uncertainty of the result. The sample variance $\text{var}[A] = \langle (A - \langle A \rangle)^2 \rangle$ associated with the Φ^2 distribution is

$$\begin{aligned} \text{var}_{\Phi^2}[A] &= \sum_{i=1}^n a_i^{(1)2} \langle u_i^2 \rangle_{\Phi^2} \\ &+ \sum_{i=1}^n a_{ii}^{(2)2} (\langle u_i^4 \rangle_{\Phi^2} - \langle u_i^2 \rangle_{\Phi^2}^2) \\ &+ \sum_{i<j}^n a_{ij}^{(2)2} \langle u_i^2 \rangle_{\Phi^2} \langle u_j^2 \rangle_{\Phi^2} \\ &+ \sum_{i=1}^n a_i^{(1)} a_{iii}^{(3)} \langle u_i^4 \rangle_{\Phi^2} \\ &+ \sum_{i<j}^n (a_i^{(1)} a_{ijj}^{(3)} + a_j^{(1)} a_{ijj}^{(3)}) \langle u_i^2 \rangle_{\Phi^2} \langle u_j^2 \rangle_{\Phi^2} \\ &+ \mathcal{O}(u^6). \end{aligned} \quad (15)$$

The expression for $\text{var}_{\Phi_{\text{TL}}^2}[A]$ is similar to Eq. 15, but replacing $\langle u_i^4 \rangle_{\Phi^2}$ with $\langle u_i^2 \rangle_{\Phi^2}^2$, which eliminates the second term. The leading order contribution to both $\text{var}_{\Phi^2}[A]$ and $\text{var}_{\Phi_{\text{TL}}^2}[A]$ is thus due to the asymmetry of the expectation value along individual modes. We note that there exist observables for which the thermal lines method gives a greater variance than direct Monte Carlo integration. For example, for a one-dimensional harmonic wave function of frequency $\omega = 1$ the function $A(u) = -3u + u^2 + u^3$ is sampled with greater variance with unsymmetrized-sampling thermal lines than with unsymmetrized-sampling direct Monte Carlo. However, in the absence of asymmetries, the cancellation of the

second term in Eq. 15 implies that $\text{var}_{\Phi_{\text{TL}}^2}[A] < \text{var}_{\Phi^2}[A]$ to leading order.

The variance of A^* can be obtained from Eq. 15 by zeroing the a coefficients of odd-order terms, so only the second and third terms survive in $\text{var}_{\Phi^2}[A^*]$, and only the third term survives in $\text{var}_{\Phi_{\text{TL}}^2}[A^*]$. Thus, the variance from symmetrized-sampling thermal lines is identically zero in one dimension, and in multiple dimensions the sample variance arises solely from multi-mode contributions. By contrast, $\text{var}_{\Phi^2}[A^*]$ contains single-mode contributions, hence $\text{var}_{\Phi_{\text{TL}}^2}[A^*] < \text{var}_{\Phi^2}[A^*]$ to leading order.

The thermal lines method combines the construction of a one-dimensional two-point integration grid with n -dimensional Monte Carlo sampling, and it is useful to analyze these two aspects of the method separately. If stochastic sampling is ignored, thermal lines reduces to quadrature integration; in fact, the thermal lines grid for the harmonic wave function is a two-point Gauss-Hermite quadrature grid.⁵¹ In the following, we generalize thermal lines by formulating one-dimensional quadrature grids adapted to the single-mode wave function in Section IV, and then we separately discuss the n -dimensional Monte Carlo sampling of these grids in Section V.

IV. ONE-DIMENSIONAL QUADRATURE GRIDS

We define our quadrature grids as an approximation to the integral

$$\langle A \rangle_{\phi^2} = \int_{-\infty}^{\infty} \phi^2(u) A(u) du \approx \sum_{\alpha=1}^p P_{\alpha} A(U_{\alpha}), \quad (16)$$

where p is the number of points in the grid, U_{α} is the α th grid point, and P_{α} is its corresponding weight, which satisfies $\sum_{\alpha=1}^p P_{\alpha} = 1$. This approximation is equivalent to replacing $\phi^2(u)$ in Eq. 16 with the discrete probability distribution

$$\psi_p^2(u) = \sum_{\alpha=1}^p P_{\alpha} \delta(u - U_{\alpha}), \quad (17)$$

so that the right-hand side of Eq. 16 is $\langle A \rangle_{\psi_p^2}$. Note that when $p \rightarrow \infty$ Eq. 17 must reduce to the full single-mode probability distribution, $\lim_{p \rightarrow \infty} P_{\alpha} \propto \phi^2(U_{\alpha})$.

A p -point quadrature grid has $2p$ unknowns, which we determine by imposing that the quadrature integral be exact for a polynomial of order $2p - 1$. Let

$$A(u) = \sum_{\beta=0}^{2p-1} a_{\beta} u^{\beta}. \quad (18)$$

The left-hand side of Eq. 16 is then

$$\langle A \rangle_{\phi^2} = \sum_{\beta=0}^{2p-1} a_{\beta} \langle u^{\beta} \rangle_{\phi^2} = \sum_{\beta=0}^{2p-1} a_{\beta} \mu_{\beta}, \quad (19)$$

where $\mu_\beta = \langle u^\beta \rangle_{\phi^2}$ is the β th moment of ϕ^2 , and the right-hand side of Eq. 16 is

$$\langle A \rangle_{\psi_p^2} = \sum_{\beta=0}^{2p-1} a_\beta \langle u^\beta \rangle_{\psi_p^2} = \sum_{\beta=0}^{2p-1} a_\beta \sum_{\alpha=1}^p P_\alpha U_\alpha^\beta. \quad (20)$$

Equating each term in the right-hand sides of Eqs. 19 and 20 yields

$$\left\{ \sum_{\alpha=1}^p P_\alpha U_\alpha^\beta = \mu_\beta \right\}_{\beta=0}^{2p-1}. \quad (21)$$

The condition that the weights be normalized corresponds to $\beta = 0$ in Eq. 21. Note that, despite being derived for polynomial integrands, quadrature grid integration can also accurately approximate integrals of functions whose Taylor expansions do not converge in the integration range, as demonstrated below.

Non-symmetric wave functions require solving the full system of equations specified by Eq. 21. Grids for symmetric wave functions must be symmetric, so if U is a grid point with weight P , then $-U$ must also be a grid point with weight P , and consequently if p is odd then $U = 0$ must be a grid point. This eliminates p equations from Eq. 21 and determines p unknowns. It is thus possible to obtain explicit analytical expressions for the grid parameters of denser grids for symmetric wave functions than for non-symmetric wave functions. In Table I we give the parameters for symmetric 2-, 3- and 4-point grids, and for the non-symmetric 2-point grid. Note that the symmetric 2-point grid corresponds to thermal lines, and the non-symmetric 2-point grid reduces to the symmetric 2-point grid if $\phi^2(u)$ has zero skewness.

Larger grids can be constructed for any vibrational wave function by numerically solving Eq. 21. In Figs. 1 and 2 we show 2- to 10-point grids obtained for a symmetric and a non-symmetric anharmonic potential, respectively. The convergence of the grid weights to the square of the vibrational wave function can be appreciated in the plots.

We test these numerical grids by integrating four test functions which can be regarded as models of the dependence of an electronic observable A on the mode amplitude u . Our test functions are a pure quadratic function, $A_1 = u^2$, a non-monotonic, non-symmetric quartic polynomial which takes negative values, $A_2 = 0.5u - u^2 + u^4$, a non-monotonic, symmetric, non-negative sixth-order polynomial, $A_3 = 2u^2 - 2.8u^4 + u^6$, and a monotonic, non-negative, non-polynomial function locally dominated by a quadratic term, $A_4 = \frac{4u^2}{1+2|u|}$. These functions are plotted in Fig. 3. Functions similar to A_2 and A_3 have been used to model band gaps in some systems,⁵² while functions with the linear asymptotic behavior of A_4 have been reported in previous studies.^{35,42}

The convergence of the variance of A is particularly relevant to the multi-dimensional Monte Carlo sampling of quadrature grids. By construction, the bias in any expectation value obtained with a p -point quadrature grid is $\mathcal{O}(u^{2p})$. Therefore, if A is a polynomial of order n_A , its quadrature grid expectation value converges to the exact value at order

ϕ^2	p	α	U_α	P_α	
Symmetric	2	1	$-\sqrt{\mu_2}$	$1/2$	
		2	$\sqrt{\mu_2}$	$1/2$	
	3	1	$-\sqrt{\frac{\mu_4}{\mu_2}}$	$\frac{\mu_2^2}{2\mu_4}$	
		2	0	$1 - \frac{\mu_2^2}{\mu_4}$	
		3	$\sqrt{\frac{\mu_4}{\mu_2}}$	$\frac{\mu_2^2}{2\mu_4}$	
	4	1	$-\sqrt{\frac{\xi_6 + \zeta_6}{2\xi_4}}$	$\frac{1}{4} - \frac{\xi_6 - 2\mu_2\xi_4}{4\zeta_6}$	
		2	$-\sqrt{\frac{\xi_6 - \zeta_6}{2\xi_4}}$	$\frac{1}{4} + \frac{\xi_6 - 2\mu_2\xi_4}{4\zeta_6}$	
		3	$\sqrt{\frac{\xi_6 - \zeta_6}{2\xi_4}}$	$\frac{1}{4} + \frac{\xi_6 - 2\mu_2\xi_4}{4\zeta_6}$	
		4	$\sqrt{\frac{\xi_6 + \zeta_6}{2\xi_4}}$	$\frac{1}{4} - \frac{\xi_6 - 2\mu_2\xi_4}{4\zeta_6}$	
	where:				
	$\xi_6 = \mu_6 - \mu_2\mu_4$				
	$\xi_4 = \mu_4 - \mu_2^2$				
$\zeta_6 = \sqrt{\xi_6^2 - 4\xi_4(\xi_6\mu_2 - \xi_4\mu_4)}$					
Non-symmetric	2	1	$-\frac{2\mu_2^2}{\mu_3 + \sqrt{\mu_3^2 + 4\mu_2^3}}$	$\frac{1}{2} + \frac{\mu_3}{2\sqrt{\mu_3^2 + 4\mu_2^3}}$	
		2	$\frac{\mu_3 + \sqrt{\mu_3^2 + 4\mu_2^3}}{2\mu_2}$	$\frac{1}{2} - \frac{\mu_3}{2\sqrt{\mu_3^2 + 4\mu_2^3}}$	

TABLE I. Analytical expressions for the grid parameters obtained by solving Eq. 21 for various grid sizes p for symmetric and non-symmetric wave functions. Grid parameters for the harmonic wave function can be obtained by substituting $\mu_2 = 1/(2\omega)$, $\mu_4 = 3\mu_2^2$, and $\mu_6 = 15\mu_2^3$ in the expressions for symmetric grid parameters. Note that we assume $\mu_1 = 0$, which can always be accomplished by working with the shifted coordinate $u' = u - \mu_1$; therefore in this table μ_β refers to the β th central moment of $\phi^2(u)$.

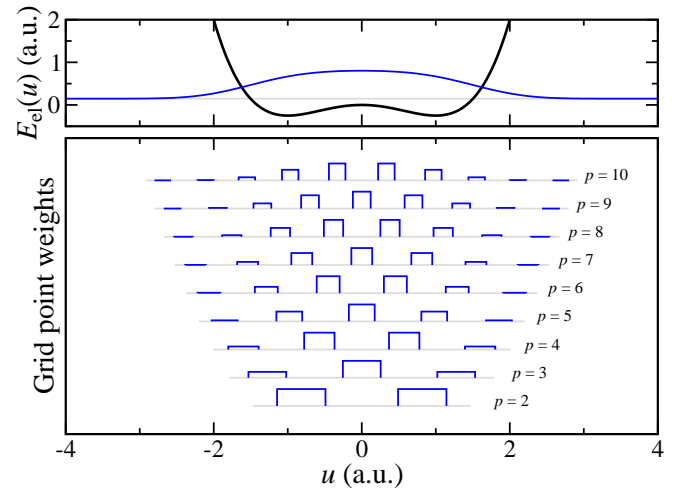


FIG. 1. Symmetric anharmonic potential $E_{\text{el}}(u) = -\frac{1}{2}u^2 + \frac{1}{4}u^4$ with its ground-state wave function (top panel), and quadrature grids constructed using this wave function (bottom panel).

$p = \lceil \frac{n_A + 1}{2} \rceil$, while the variance of A is a polynomial of order $2n_A$ and its quadrature grid estimate converges to the exact

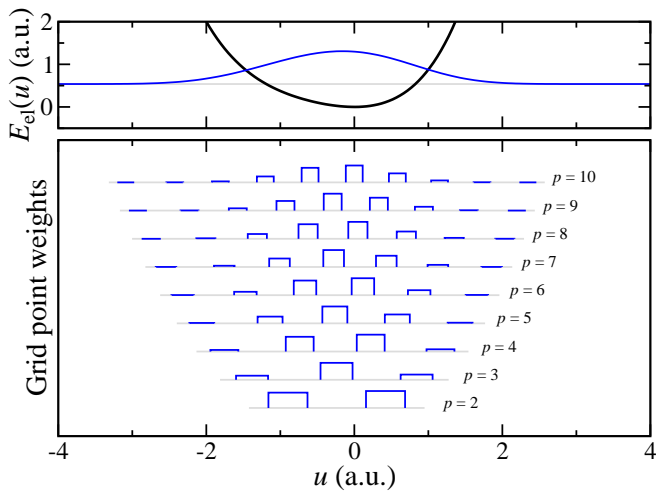


FIG. 2. Non-symmetric anharmonic potential $E_{\text{el}}(u) = \frac{1}{2}u^2 + \frac{1}{4}u^3 + \frac{1}{8}u^4$ with its ground-state wave function (top panel), and quadrature grids constructed using this wave function (bottom panel).

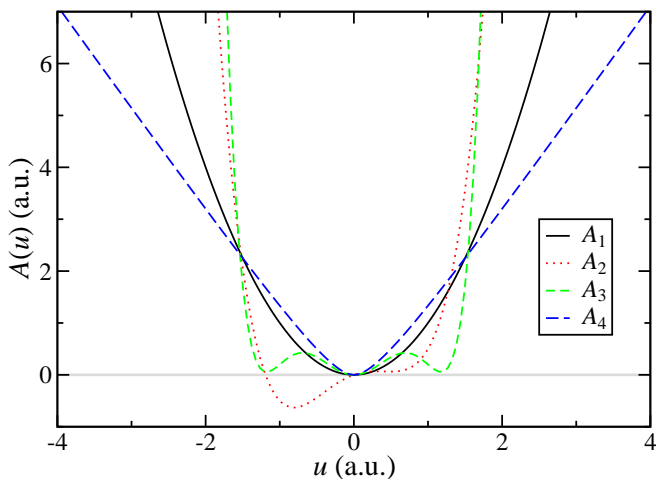


FIG. 3. Test functions $A_1 = u^2$, $A_2 = 0.5u - u^2 + u^4$, $A_3 = 2u^2 - 2.8u^4 + u^6$, and $A_4 = \frac{4u^2}{1+2|u|}$, which serve as models of the dependence of an electronic observable A on mode amplitude u .

variance at $p = n_A + 1$. Thus, if the variance approaches its exact value monotonically from below, it would be possible to obtain the exact expectation value of A with a smaller uncertainty than with direct Monte Carlo by stochastically sampling a quadrature grid of $\lceil \frac{n_A+1}{2} \rceil \leq p < n_A + 1$ points. Knowledge of n_A for any given expectation value would then allow selecting the grid size $p = \lceil \frac{n_A+1}{2} \rceil$ that maximizes the efficiency of the stochastic sampling and incurs zero bias.

In Figs. 4 and 5 we plot the expectation value and variance of the four test functions for the symmetric and non-symmetric numerical grids, respectively. In these tests, the integrals of polynomials of order n_A are approximated particularly poorly by grids with $p < \lceil \frac{n_A+1}{2} \rceil$ points. For $\lceil \frac{n_A+1}{2} \rceil \leq p < n_A + 1$ the quadrature integrals are exact, as expected, while the variance approaches its exact value from

below, making stochastic quadrature grid integration advantageous over direct Monte Carlo at these grid sizes.

The expectation value and variance of the non-polynomial A_4 test function converge slowly and non-monotonically to their respective exact values, but the quadrature integrals of A_4 are reasonably good approximations to the exact integral at all p , and two-point grids are particularly efficient since the corresponding variances are small (or indeed, zero for a symmetric wave function).

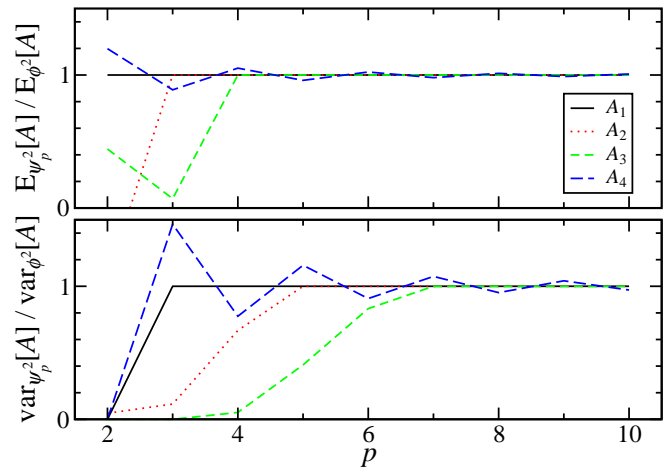


FIG. 4. Quadrature-grid expectation value (top panel) and variance (bottom panel) of each of the four test functions plotted in Fig. 3 relative to the exact expectation value and variance, respectively, as a function of the number of points p in the symmetric grids plotted in Fig. 1.

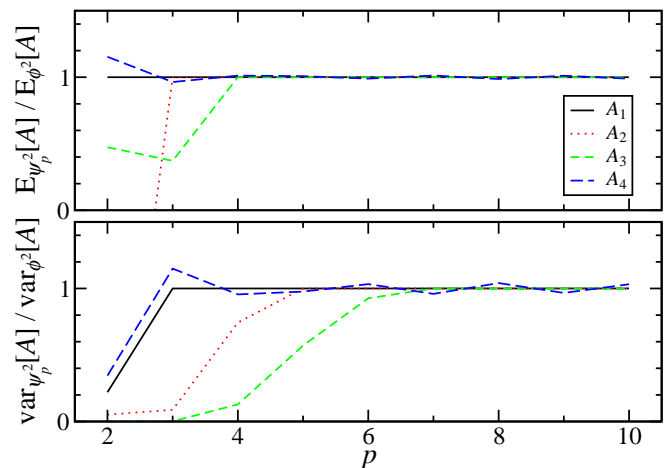


FIG. 5. Quadrature-grid expectation value (top panel) and variance (bottom panel) of each of the four test functions plotted in Fig. 3 relative to the exact expectation value and variance, respectively, as a function of the number of points p in the non-symmetric grids plotted in Fig. 2.

V. n -DIMENSIONAL MONTE CARLO SAMPLING OF ONE-DIMENSIONAL QUADRATURE GRIDS

We define quadrature grids for each of the n normal-mode coordinates, which are stochastically sampled by choosing random grid points with probability proportional to their weights. The basic properties of expectation values of functions of n variables differ from those in one dimension due to the effect of multi-mode contributions. As in the case of thermal lines, n -dimensional sampling of p -point quadrature grids correctly accounts for multi-mode contributions to the expectation value involving up to the $(2p - 1)$ th power of normal-mode coordinates, exceeding the order to which single-mode contributions are exact. Therefore we do not expect major differences in the behavior and convergence properties of n -dimensional quadrature grid expectation values with respect to the one-dimensional case.

Observables along most of the normal modes in a system are found in practice to be strongly quadratic, and therefore it is particularly interesting to investigate the use of per-mode grid sizes adapted to the specific system under consideration. We test n -dimensional sampling of quadrature grids by evaluating the zero-point correction to the band gap of a primitive cell of the HF and NH₃ molecular crystals using the harmonic vibrational wave function. These systems were found to be particularly problematic under the quadratic approximation in Ref. 35, and therefore our results should be representative of the usefulness of multi-point quadrature grids in difficult cases. The band gap of HF is a markedly non-quadratic function of the highest-frequency normal mode, similar in shape to the one-dimensional test function A_4 in Section IV, see Fig. 2 of Ref. 35, while it is found to be a strongly quadratic function of the 20 remaining normal modes. We similarly find that the non-quadratic behavior of the band gap of NH₃ arises largely from two mid-frequency normal modes, with the 43 remaining modes providing mostly quadratic contributions. This information allows us to choose which normal modes to sample using grids of $p > 2$ points.

The local value of the band gap at each nuclear configuration is evaluated using the plane-wave DFT method with the PBE functional⁵³ as implemented in the CASTEP code,⁵⁴ and vibrational calculations are performed using our own code. We use symmetrized sampling for all of our calculations, and we test (i) varying the number of grid points along all normal modes, and (ii) varying the number of grid points only along the modes for which we find the band gap to be non-quadratic, using two-point grids for the remaining modes. The expectation value and variance of the band gap of HF and NH₃ are plotted in Figs. 6 and 7, respectively, as a function of the number of points p in the integration grid.

The results using p grid points along all normal modes converge quickly towards the infinite grid limit. The sample variance is within statistical uncertainty of this limit for $p \geq 3$, implying that, while quadrature grids with $p > 2$ offer excellent results for these systems, they offer no speed advantage over direct Monte Carlo integration. Only two-point grids (thermal lines) provide a significant reduction in statistical uncertainty, while still improving upon the quadratic approximation thanks

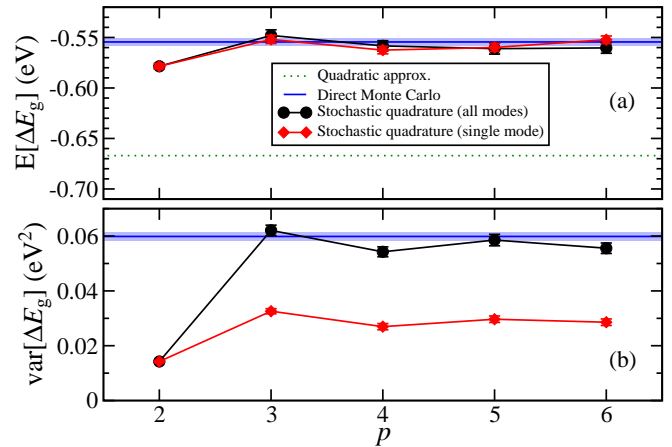


FIG. 6. (a) expectation value and (b) sample variance of the zero-point correction to the band gap of a primitive cell of the HF molecular crystal as a function of the grid size along all normal modes (black circles) and only along the mode for which the band gap is found to be non-quadratic, with the remaining modes using two-point grids (red diamonds). The horizontal blue lines represent the exact results evaluated by direct Monte Carlo integration, the light-colored areas represent their standard errors, and the horizontal green dotted line is the expectation value obtained with the quadratic approximation.

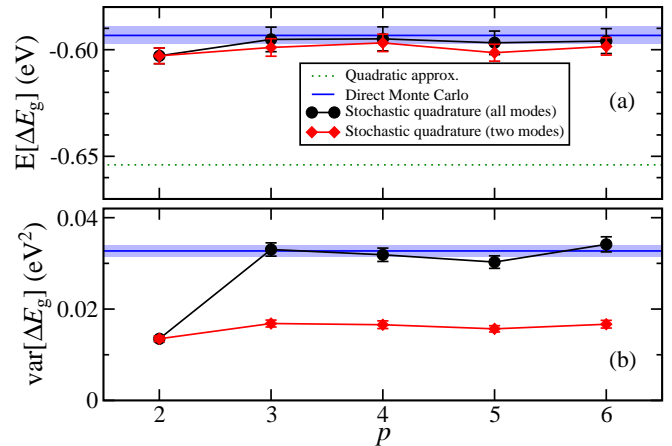


FIG. 7. (a) expectation value and (b) sample variance of the zero-point correction to the band gap of a primitive cell of the NH₃ molecular crystal as a function of the grid size along all normal modes (black circles) and only along the two modes for which the band gap is found to be non-quadratic, with the remaining modes using two-point grids (red diamonds). The horizontal blue lines represent the exact results evaluated by direct Monte Carlo integration, the light-colored areas represent their standard errors, and the horizontal green dotted line is the expectation value obtained with the quadratic approximation.

to correctly accounting for multi-mode contributions.

In the case of the HF molecular crystal, limiting the use of grids with $p > 2$ points to the normal mode of which the band gap is a non-quadratic function gives expectation values within statistical uncertainty of the direct Monte Carlo result, but with about half the sample variance. This implies a $\sim 30\%$ reduction in the number of samples needed to obtain the ex-

pectation value to a target statistical uncertainty. For NH_3 the uncertainty in the expectation value of the band gap prevents drawing strong conclusions regarding the selective application of multi-point grids, but the results hint at a reduced bias compared with $p = 2$, and the sample variance is again about half that obtained with direct Monte Carlo.

These results reflect that, even when non-quadratic behavior is present in an observable, the overall weight of non-quadratic contributions to the result is typically small; two-point grids provide a very good approximation for quadratic contributions, and multi-point grids can be used along specific modes to avoid any bias.

VI. CONCLUSIONS

We have quantified the bias incurred by the thermal lines method, which includes higher-order terms than the quadratic approximation, and we have reformulated thermal lines as a particular choice of grid size in a stochastic implementation of quadrature grid integration. We have demonstrated the construction of one-dimensional quadrature grids adapted to specific anharmonic wave functions and their application to the integration of functions modelling the dependence of electronic observables on nuclear configurations.

The accuracy of quadrature integration ultimately depends on the function being integrated. Our tests with model polynomials show that small grid sizes can incur a large bias, but knowledge of the order of the polynomial allows exploiting the slow convergence of the variance with grid size to obtain accurate expectation values with little statistical noise.

Our tests using DFT data indicate that observables of in-

terest tend to be dominated by quadratic contributions, for which two-point grids (thermal lines) are ideally suited. However examples have been reported of observables with strong non-quadratic components along specific modes,^{35,42,52} and we find that selectively using quadrature grids with three or more points along these modes eliminates the bias in the expectation values.

We therefore recommend that the behavior of observables along each normal mode be determined prior to the application of stochastic quadrature grid integration in order to select the optimal grid size and avoid incurring a bias. This type of analysis can be trivially performed during the mapping of the Born-Oppenheimer energy surface $E_{\text{el}}(\mathbf{u})$ involved in solving anharmonic vibrational Hamiltonians, and can be carried out separately by direct inspection when using the harmonic approximation.

ACKNOWLEDGMENTS

P.L.R. acknowledges financial support from the Max-Planck Society. R.J.N. acknowledges financial support from the Engineering and Physical Sciences Research Council, U.K., under grant no. EP/P034616/1. B.M. acknowledges Robinson College, Cambridge, and the Cambridge Philosophical Society for a Henslow Research Fellowship. We are grateful for computational support from the UK national high performance computing service, ARCHER, for which access was obtained via the UKCP consortium and funded by EPSRC grant no. EP/P022561/1. Supporting research data may be freely accessed at [URL], in compliance with the applicable Open Data policies.

* pl275@cam.ac.uk

¹ M. Born and R. Oppenheimer, *Zur Quantentheorie der Molekeln*, *Ann. Phys.* **389**, 457 (1927).

² R.O. Jones, *Density functional theory: Its origins, rise to prominence, and future*, *Rev. Mod. Phys.* **87**, 897 (2015).

³ L. Hedin, *New Method for Calculating the One-Particle Green's Function with Application to the Electron-Gas Problem*, *Phys. Rev.* **139**, A796 (1965).

⁴ F. Aryasetiawan and O. Gunnarsson, *The GW method*, *Rep. Prog. Phys.* **61**, 237 (1998).

⁵ D. M. Ceperley and B. J. Alder, *Ground State of the Electron Gas by a Stochastic Method*, *Phys. Rev. Lett.* **45**, 566 (1980).

⁶ W. M. C. Foulkes, L. Mitas, R. J. Needs, and G. Rajagopal, *Quantum Monte Carlo simulations of solids*, *Rev. Mod. Phys.* **73**, 33 (2001).

⁷ D. C. Wallace, *Thermodynamics of Crystals* (John Wiley & Sons, New York, 1972).

⁸ M. Born and K. Huang, *Dynamical Theory of Crystal Lattices* (Oxford University Press, Oxford, 1956).

⁹ A. A. Maradudin, E. W. Montroll, G. H. Weiss, and I. P. Ipatova, *Theory of Lattice Dynamics in the Harmonic Approximation*, 2nd ed. (Academic Press, New York, 1971).

¹⁰ I. Errea, M. Calandra, C. J. Pickard, J. R. Nelson, R. J. Needs, Y. Li, H. Liu, Y. Zhang, Y. Ma, and F. Mauri, *Quantum hydrogen-*

bond symmetrization in the superconducting hydrogen sulfide system, *Nature* **532**, 81 (2016).

¹¹ C. W. Li, X. Tang, J. A. Muñoz, J. B. Keith, S. J. Tracy, D. L. Abernathy, and B. Fultz, *Structural Relationship between Negative Thermal Expansion and Quartic Anharmonicity of Cubic ScF_3* , *Phys. Rev. Lett.* **107**, 195504 (2011).

¹² L.-D. Zhao, S.-H. Lo, Y. Zhang, H. Sun, G. Tan, C. Uher, C. Wolverton, V. P. Dravid, and M. G. Kanatzidis, *Ultralow thermal conductivity and high thermoelectric figure of merit in SnSe crystals*, *Nature* **508**, 373 (2014).

¹³ J. Trail, B. Monserrat, P. López Ríos, R. Maezono, and R. J. Needs, *Quantum Monte Carlo study of the energetics of the rutile, anatase, brookite, and columbite TiO_2 polymorphs*, *Phys. Rev. B* **95**, 121108(R) (2017).

¹⁴ D. J. Hooton, *The use of a model in anharmonic lattice dynamics*, *Philos. Mag.* **3**, 49 (1958).

¹⁵ P. Souvatzis, O. Eriksson, M. I. Katsnelson, and S. P. Rudin, *Entropy driven stabilization of energetically unstable crystal structures explained from first principles theory*, *Phys. Rev. Lett.* **100**, 095901 (2008).

¹⁶ O. Hellman, I. A. Abrikosov, and S. I. Simak, *Lattice dynamics of anharmonic solids from first principles*, *Phys. Rev. B* **84**, 180301 (2011).

¹⁷ N. Antolin, O. D. Restrepo, and W. Windl, *Fast free-*

- energy calculations for unstable high-temperature phases, *Phys. Rev. B* **86**, 054119 (2012).
- ¹⁸ B. Monserrat, N. D. Drummond, and R. J. Needs, *Anharmonic vibrational properties in periodic systems: Energy, electron-phonon coupling, and stress*, *Phys. Rev. B* **87**, 144302 (2013).
- ¹⁹ I. Errea, M. Calandra, and F. Mauri, *First-principles theory of anharmonicity and the inverse isotope effect in superconducting palladium-hydride compounds*, *Phys. Rev. Lett.* **111**, 177002 (2013).
- ²⁰ P. B. Allen and V. Heine, *Theory of the temperature dependence of electronic band structures*, *J. Phys. C* **9**, 2305 (1976).
- ²¹ P. B. Allen and M. Cardona, *Theory of the temperature dependence of the direct gap of germanium*, *Phys. Rev. B* **23**, 1495 (1981).
- ²² F. Giustino, S. G. Louie, and M. L. Cohen, *Electron-Phonon Renormalization of the Direct Band Gap of Diamond*, *Phys. Rev. Lett.* **105**, 265501 (2010).
- ²³ F. E. Williams, *Theoretical low temperature spectra of the thallium activated potassium chloride phosphor*, *Phys. Rev.* **82**, 281 (1951).
- ²⁴ M. Lax, *The Franck-Condon principle and its application to crystals*, *J. Chem. Phys.* **20**, 1752 (1952).
- ²⁵ C. E. Patrick and F. Giustino, *Unified theory of electron-phonon renormalization and phonon-assisted optical absorption*, *J. Phys.: Condens. Matter* **26**, 365503 (2014).
- ²⁶ M. Zacharias, C. E. Patrick, and F. Giustino, *Stochastic Approach to Phonon-Assisted Optical Absorption*, *Phys. Rev. Lett.* **115**, 177401 (2015).
- ²⁷ S. Rossano, F. Mauri, C. J. Pickard, and I. Farnan, *First-Principles Calculation of ^{17}O and ^{25}Mg NMR Shieldings in MgO at Finite Temperature: Rovibrational Effect in Solids*, *J. Phys. Chem. B* **109**, 7245 (2005).
- ²⁸ J. N. Dumez and C. J. Pickard, *Calculation of NMR chemical shifts in organic solids: Accounting for motional effects*, *J. Chem. Phys.* **130**, 104701 (2009).
- ²⁹ B. Monserrat, R. J. Needs, and C. J. Pickard, *Temperature effects in first-principles solid state calculations of the chemical shielding tensor made simple*, *J. Chem. Phys.* **141**, 134113 (2014).
- ³⁰ M. Dračinský and P. Hodgkinson, *Effects of Quantum Nuclear Delocalisation on NMR Parameters from Path Integral Molecular Dynamics*, *Chem. Eur. J.* **20**, 2201 (2014).
- ³¹ R. Nemausat, D. Cabaret, C. Gervais, C. Brouder, N. Trcera, A. Bordage, I. Errea, and F. Mauri, *Phonon effects on x-ray absorption and nuclear magnetic resonance spectroscopies*, *Phys. Rev. B* **92**, 144310 (2015).
- ³² A. R. Porter, M. D. Towler, and R. J. Needs, *Muonium as a hydrogen analogue in silicon and germanium: Quantum effects and hyperfine parameters*, *Phys. Rev. B* **60**, 13534 (1999).
- ³³ J. S. Möller, D. Ceresoli, T. Lancaster, N. Marzari, and S. J. Blundell, *Quantum states of muons in fluorides*, *Phys. Rev. B* **87**, 121108(R) (2013).
- ³⁴ B. Monserrat, N. D. Drummond, C. J. Pickard, and R. J. Needs, *Electron-Phonon Coupling and the Metallization of Solid Helium at Terapascal Pressures*, *Phys. Rev. Lett.* **112**, 055504 (2014).
- ³⁵ B. Monserrat, E. A. Engel, and R. J. Needs, *Giant electron-phonon interactions in molecular crystals and the importance of nonquadratic coupling*, *Phys. Rev. B* **92**, 140302 (2015).
- ³⁶ C. E. Patrick, K. W. Jacobsen, and K. S. Thygesen, *Anharmonic stabilization and band gap renormalization in the perovskite CsSnI₃*, *Phys. Rev. B* **92**, 201205(R) (2015).
- ³⁷ W. A. Saidi, S. Poncé, and B. Monserrat, *Temperature dependence of the energy levels of methylammonium lead iodide perovskite from first principles*, *J. Phys. Chem. Lett.* **7**, 5247 (2016).
- ³⁸ B. Monserrat, *Vibrational averages along thermal lines*, *Phys. Rev. B* **93**, 014302 (2016).
- ³⁹ K. Kunc and R. M. Martin, *Ab Initio Force Constants of GaAs: A New Approach to Calculation of Phonons and Dielectric Properties*, *Phys. Rev. Lett.* **48**, 406 (1982).
- ⁴⁰ J. H. Lloyd-Williams and B. Monserrat, *Lattice dynamics and electron-phonon coupling calculations using nondiagonal supercells*, *Phys. Rev. B* **92**, 184301 (2015).
- ⁴¹ S. Baroni, S. de Gironcoli, A. Dal Corso, and P. Giannozzi, *Phonons and related crystal properties from density-functional perturbation theory*, *Rev. Mod. Phys.* **73**, 515 (2001).
- ⁴² G. Antonius, S. Poncé, E. Lantagne-Hurtubise, G. Auclair, X. Gonze, and M. Côté, *Dynamical and anharmonic effects on the electron-phonon coupling and the zero-point renormalization of the electronic structure*, *Phys. Rev. B* **92**, 085137 (2015).
- ⁴³ A. Baldereschi, *Mean-Value Point in the Brillouin Zone*, *Phys. Rev. B* **7**, 5212 (1973).
- ⁴⁴ G. Rajagopal, R. J. Needs, S. Kenny, W. M. C. Foulkes, and A. James, *Quantum Monte Carlo Calculations for Solids Using Special k Points Methods*, *Phys. Rev. Lett.* **73**, 1959 (1994).
- ⁴⁵ V. I. Lebedev, *Quadratures on a sphere*, *Zh. vychisl. Mat. mat. Fiz.* **16**, 293 (1976).
- ⁴⁶ J. A. Reeger and B. Fornberg, *Numerical Quadrature over the Surface of a Sphere*, *Stud. Appl. Math.* **137**, 174 (2015).
- ⁴⁷ B. Monserrat, *Correlation effects on electron-phonon coupling in semiconductors: Many-body theory along thermal lines*, *Phys. Rev. B* **93**, 100301(R) (2016).
- ⁴⁸ B. Monserrat, C. E. Dreyer, and K. M. Rabe, *Phonon-assisted optical absorption in BaSnO₃ from first principles*, [arXiv:1709.09196](https://arxiv.org/abs/1709.09196).
- ⁴⁹ M. Zacharias and F. Giustino, *One-shot calculation of temperature-dependent optical spectra and phonon-induced band-gap renormalization*, *Phys. Rev. B* **94**, 075125 (2016).
- ⁵⁰ M. Komelj and H. Krakauer, *Electron-phonon coupling and exchange-correlation effects in superconducting H₃S under high pressure*, *Phys. Rev. B* **92**, 205125 (2015).
- ⁵¹ M. Abramowitz and I. A. Stegun, editors, *Handbook of Mathematical Functions* (Dover Publications Incorporated, New York, 1972).
- ⁵² L. D. Whalley, J. M. Skelton, J. M. Frost, and A. Walsh, *Phonon anharmonicity, lifetimes, and thermal transport in CH₃NH₃PbI₃ from many-body perturbation theory*, *Phys. Rev. B* **94**, 220301 (2016).
- ⁵³ J. P. Perdew, K. Burke, and M. Ernzerhof, *Generalized Gradient Approximation Made Simple*, *Phys. Rev. Lett.* **77**, 3865 (1996); Erratum *Phys. Rev. Lett.* **78**, 1396(E) (1997).
- ⁵⁴ S. J. Clark, M. D. Segall, C. J. Pickard, P. J. Hasnip, M. I. J. Probert, K. Refson, and M. C. Payne, *First principles methods using CASTEP*, *Z. Kristallogr.* **220**, 567 (2005).